ACS SENSORS

pubs.acs.org/acssensors Article

Booster, a Red-Shifted Genetically Encoded Förster Resonance Energy Transfer (FRET) Biosensor Compatible with Cyan Fluorescent Protein/Yellow Fluorescent Protein-Based FRET Biosensors and Blue Light-Responsive Optogenetic Tools

Tetsuya Watabe, Kenta Terai,* Kenta Sumiyama, and Michiyuki Matsuda

Cite This: https://dx.doi.org/10.1021/acssensors.9b01941 Read Online

ACCESS | Metrics & More | Article Recommendations | Supporting Information

ABSTRACT: Genetically encoded Förster resonance energy transfer (FRET)-based biosensors have been developed for the visualization of signaling molecule activities. Currently, most of them are comprised of cyan and yellow fluorescent proteins (CFP and YFP), precluding the use of multiple FRET biosensors within a single cell. Moreover, the FRET biosensors based on CFP and YFP are incompatible with the optogenetic tools that operate at blue light. To overcome these problems, here, we have developed FRET biosensors with red-shifted excitation and emission wavelengths. We chose mKOκ and mKate2 as the favorable donor and acceptor pair by calculating the Förster distance. By optimizing the order of fluorescent proteins and modulatory domains of the FRET biosensors, we developed a FRET biosensor backbone named "Booster". The performance of the protein kinase A (PKA) biosensor based on the Booster backbone (Booster-PKA) was comparable to that of AKAR3EV, a previously developed FRET biosensor comprising CFP and YFP. For the proof of concept, we first showed simultaneous monitoring of activities of two protein kinases with Booster-PKA and ERK FRET biosensors based on CFP and YFP. Second, we showed monitoring of PKA activation by *Beggiatoa* photoactivated adenylyl cyclase, an optogenetic generator of cyclic AMP. Finally, we presented PKA activity in living tissues of transgenic mice expressing Booster-PKA. Collectively, the results demonstrate the effectiveness and versatility of Booster biosensors as an imaging tool in vitro and in vivo.

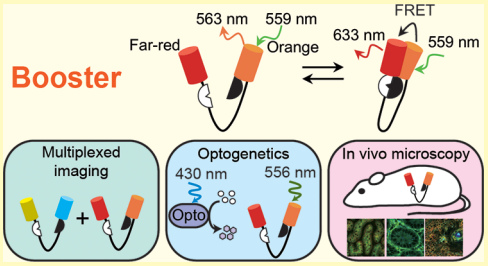

KEYWORDS: *FRET biosensor, multiplexed imaging, optogenetics, in vivo microscopy, transgenic mouse*

INTRODUCTION

Förster (or fluorescence) resonance energy transfer (FRET) is a process of nonradiative energy transfer between donor and acceptor fluorophores.[1] Genetically encoded biosensors based on the principles of FRET have been contributing to our understanding of the spatiotemporal dynamics of signaling molecules such as ions, small GTPases, and protein kinases.[2,3] Currently, the most widely used fluorescent protein (FP) pairs for the FRET biosensors are cyan FP/yellow FP (CFP/YFP) pairs.[3,4] Such CFP/YFP-based FRET biosensors use blue light for excitation, hampering the use of flavoprotein-derived optogenetic tools such as the photolyase homology region (PHR) domain of *Arabidopsis* cryptochrome 2 (CRY2), the light oxygen voltage (LOV) domain of *Avena sativa* phototropin 1, and the blue light receptor using the FAD (BLUF) domain of *Beggiatoa* photoactivated adenylyl cyclase (bPAC), all of which are activated by blue light.[5−7] Furthermore, there has been a continuing demand to monitor two signaling molecules simultaneously, leading many research groups to develop FRET biosensors with red-shifted excitation and emission wavelengths.

To use the orange to far-red wavelength range, Ouyang et al. developed an MT1-MMP biosensor comprising mOrange and mCherry as the donor and acceptor proteins, respectively.[8] Since their report, many additional FRET biosensors based on the orange to far-red wavelength range have already been reported.[9−11] However, in comparison to the CFP/YFP-based FRET biosensors, the dynamic ranges of these FRET biosensors with red-shifted fluorescent proteins are low, probably due to the spectral overlap between the donor and acceptor fluorophores[4] and/or the low quantum yields of acceptor fluorescent proteins.[12] Recently, infrared fluorescent protein (iRFP)-based FRET biosensors that allow for clear separation of signals from the CFP/YFP pair were also reported.[13−15] The quantum yields of the iRFPs are markedly lower than that of YFP, leaving room for extensive improvement.[16] An alternative approach for dual FRET imaging is to

Received: October 2, 2019
Accepted: February 14, 2020

https://dx.doi.org/10.1021/acssensors.9b01941
ACS Sens. XXXX, XXX, XXX−XXX

use donor fluorescent proteins with large Stokes shift,[17,18] although such FRET biosensors are still incompatible with flavoprotein-derived light sensors. Grant et al. reported dual FRET imaging with CFP/YFP and TagRFP/mPlum pairs by fluorescence lifetime imaging microscopy (FLIM).[19] The acquisition of FLIM-FRET images requires instruments for lifetime measurement, which may hamper widespread use of this technique among researchers.

Here, we report genetically encoded FRET biosensors with red-shifted excitation and emission wavelength. We first selected mKOκ and mKate2 as a FRET pair by calculating the Förster distance and then optimized the order of components. As the first example, we developed a FRET biosensor for protein kinase A (PKA). The performance of this new PKA biosensor, named "Booster-PKA", was comparable with that of the CFP/YFP-based PKA biosensor. As anticipated, Booster-PKA was compatible with CFP/YFP-based FRET biosensors and optogenetic manipulations. We further extended the same approach to develop FRET biosensors for other protein kinases. Finally, we generated transgenic mice expressing Booster-PKA and succeeded in intravital PKA activity imaging under a two-photon excitation microscope (TPEM).

RESULTS

Generation of FRET Biosensors Comprising Orange and Far-Red Fluorescent Proteins. To develop FRET biosensors that are compatible with the CFP/YFP-based FRET biosensors, we chose mKate2[20] as an acceptor fluorophore because it has the highest quantum yield (QY) among seven candidate far-red fluorescent proteins[16,20−23] (Figure S1A). It is known that high QY of the acceptor protein increases the sensitized emission and therefore improves the signal-to-noise ratio.[4,12] Next, we calculated the Förster distance between mKate2 and seven candidates for the donor fluorescent protein[24−29] (Figure S1B,C) and chose mKOκ[27] because it has the longest Förster distance. The first biosensor was based on a variant of AKAR3EV,[30] which consists of Turquoise-GL,[31] an FHA1 phosphothreonine-binding domain, a 116-amino-acid flexible EV linker, a PKA substrate peptide, and YPet[32] (Figure 1A). In this paper, we describe this variant as AKAR3EV. The prototype biosensor #1 was constructed simply by replacing Turquoise-GL and YPet with mKOκ and mKate2, respectively. Then, in an effort to obtain a high-performance sensor, we shuffled the order of the fluorescent proteins, FHA1 domain, and substrate domain under the constraint that the fluorescent proteins must be separated by the EV linker. We used FLIM for the validation of FRET biosensors because FLIM is highly quantitative and reproducible. These 16 biosensors were expressed in HeLa cells and imaged by FLIM. The fluorescence lifetime of mKOκ before and after the addition of an adenylyl cyclase activator, forskolin, was measured to calculate the decrease in fluorescence lifetime (Figure S2A,B). Biosensor #2 exhibited the largest decrease in lifetime, 0.67 ± 0.09 ns (Figure 1A). This is equivalent to a 21.2% change in FRET efficiency based on the fluorescence lifetime of mKOκ, 3.17 ± 0.03 ns. Of note, forskolin stimulation induced aggregation of biosensors #7, #10, and #11, which excluded these biosensors from further analysis (Figure S2A).

We previously reported that the flexible long linker increases the dynamic range by reducing FRET efficiency in the OFF state.[30] Therefore, we increased the length of the linker to 244

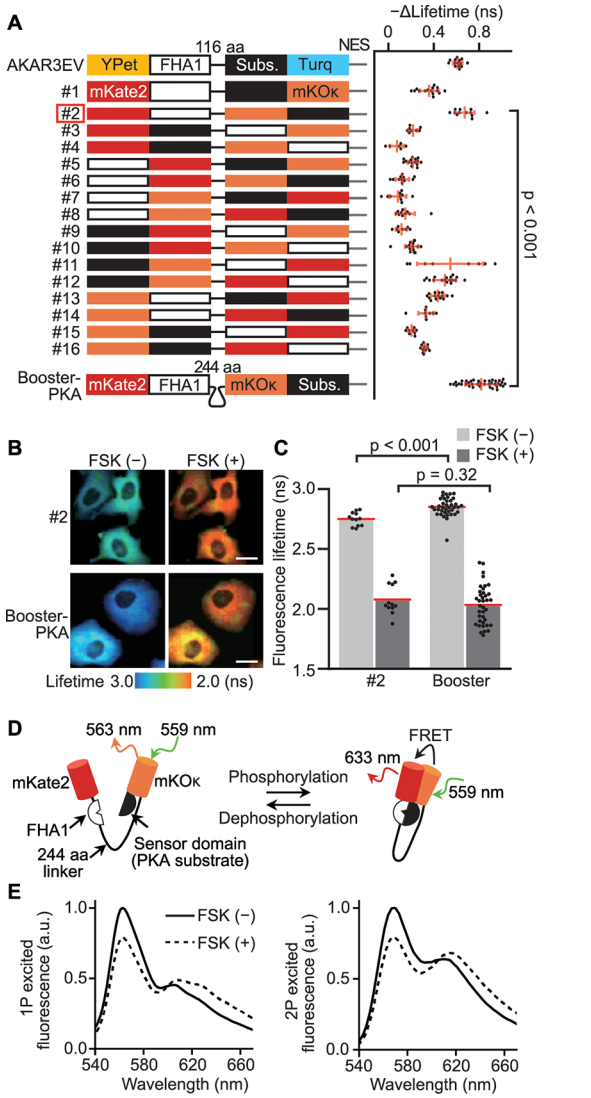

Figure 1. Development of the red-shifted FRET biosensor Booster. (A) Construction and evaluation of the red-shifted FRET biosensors. The prototype PKA biosensor AKAR3EV consists of, from the N-terminus, YPet, FHA1 (white box), a 116-amino-acid EV linker, substrate (black box), Turquoise-GL (Turq), and nuclear export signal (NES). Sensors #1−#16 were generated by shuffling the positions of mKate2, mKOκ, FHA1, and substrate. Booster-PKA is a derivative of #2 with a 244-amino-acid linker. These FRET biosensors were expressed in HeLa cells. The fluorescence lifetime of Turquoise-GL or mKOκ in each cell was measured by FLIM. Decreases in the fluorescence lifetime 10 min after the addition of forskolin (FSK; 50 μM) are shown in the right panel. Plots indicate the decreases in the lifetime of each cell, and red bars are means and SD. For each biosensor, data are obtained from more than six cells from a single experiment. The *p*-value was calculated by unpaired two-tailed Welch's *t*-test. (B, C) Representative lifetime images and quantified results of biosensor #2 and Booster-PKA expressed in HeLa cells before and 10 min after 50 μM FSK stimulation. Scale bars, 20 μm. Red bars are means. For biosensor #2, 12 cells from a single experiment were used, and for Booster-PKA, 38 cells from four independent experiments were used. The *p*-values were calculated by unpaired two-tailed Welch's *t*-test. (D) Mode of action of Booster-PKA. (E) Normalized emission profiles of Booster-PKA obtained by single-photon (1P) or two-photon (2P) excitation. Solid and dashed curves are the data before and 10 min after the addition of 50 μM FSK, respectively.

https://dx.doi.org/10.1021/acssensors.9b01941
ACS Sens. XXXX, XXX, XXX−XXX

amino acids. As anticipated, this 244-amino-acid linker increased the lifetime in the OFF state and improved the dynamic range (Figure 1B,C), resulting in a significantly large decrease in lifetime after stimulation compared with #2 (Figure 1A). We named this novel biosensor backbone "Booster" (Figure 1D). Last, we obtained the emission spectrum to confirm that Booster-PKA can be used for the ratiometric FRET measurement (Figure 1E). HeLa cells expressing Booster-PKA were stimulated by single-photon (1P) excitation at 470 nm or two-photon (2P) excitation at 1000 nm to obtain the fluorescence emission spectra. Based on these spectra, the emission intensity at 633 nm versus that at 563 nm was used to monitor FRET change. The emission ratio was smaller upon two-photon excitation than single-photon excitation because of the cross-excitation of mKate2. This cross-excitation effect was also likely the reason why the emission ratio change by single photon excitation, 75%, was larger than that by two-photon excitation, 57%.

The success of Booster prompted us to examine whether the order of components similar to biosensor #2 could improve the performance of biosensors comprising other fluorescent proteins. First, we tested another long-wavelength FP pair, mScarlet and E2-Crimson,[23,28] and found that the design of biosensor #2, 4375NES, worked better than the AKAR3EV design, 4357NES (Figure S3). Moreover, the long linker variant, 4415NES, marked a larger decrease in lifetime than 4375NES. We also tried using Turquoise-GL and YPet. However, the design of biosensor #2, 4414NES, responded to forskolin much less efficiently than did AKAR3EV (Figure S4). Thus, the best order of the domains differs in a manner dependent on the fluorescent protein pairs used for each fluorescent protein.

Performance of Booster-PKA in FRET Ratio Imaging. Next, we compared the performance, based on the gain[30] and signal-to-noise ratio, of Booster-PKA with that of AKAR3EV in FRET ratio imaging. The "gain" is the relative increase in acceptor/donor ratio after stimulation and is expressed as a percentage of the acceptor/donor value before stimulation. Upon stimulation with forskolin, the rapid and robust increase in FRET ratio was observed in the HeLa cells expressing Booster-PKA and AKAR3EV but not the phosphorylation-deficient TA mutant (threonine to alanine within the substrate domain), Booster-PKA (TA) (Figure 2A,B). HeLa cells expressing Booster-PKA exhibited a larger gain than those expressing AKAR3EV, 79 ± 20% versus 55 ± 14% (Figure 2C). The signal-to-noise ratios did not differ significantly (Figure 2D). Overall, these results show that Booster-PKA and AKAR3EV exhibit comparable performance for the monitoring of PKA activity in sensitized FRET imaging.

Expansion of Booster to Protein Kinases. We next applied the Booster backbone to the development of biosensors for JNK, ROCK, and ERK, named Booster-JNK, Booster-ROCK, and Booster-ERK, respectively. The difference among the Booster sensors was limited to the substrate peptide and/or the phosphothreonine-binding domain, which were used in the corresponding CFP/YFP-based biosensors.[30,33−35] We treated HeLa cells expressing the Booster biosensors with stimulators and/or an inhibitor and observed their responses. Upon the addition of anisomycin, Booster-JNK exhibited a gain of 38 ± 11% (Figure 3A). Likewise, upon epidermal growth factor (EGF) stimulation, Booster-ROCK displayed a gain of 25 ± 3% (Figure 3B). This increase was abrogated upon administration of the ROCK inhibitor Y-27632.

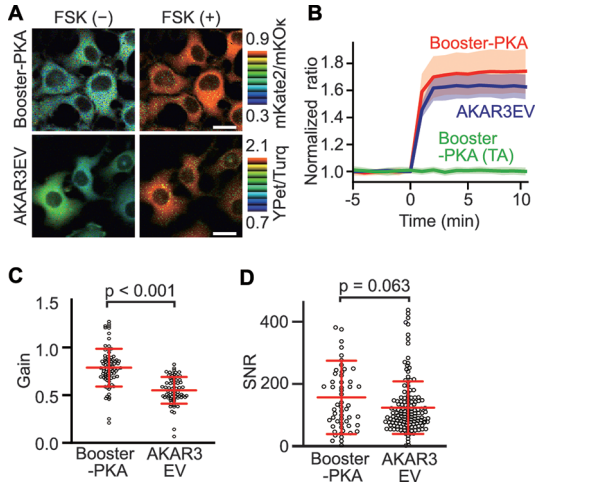

Figure 2. Comparison of Booster-PKA and AKAR3EV in the gain and signal-to-noise ratio. (A) HeLa cells expressing AKAR3EV or Booster-PKA were time lapse-imaged and stimulated with 50 μM forskolin (FSK). Representative ratio images are shown in the IMD mode. Scale bars, 20 μm. (B) Time course of emission ratios normalized at time 0. Solid lines represent the means; shaded areas represent SD. (C) Gains of emission ratio in FSK-treated HeLa cells. Plots indicate the gains of each cell, and red bars are means and SD. For Booster-PKA, 85 cells from four experiments were used, and for AKAR3EV, 72 cells from three experiments were used. The p-value was calculated by unpaired two-tailed Welch's t-test. (D) Signal-to-noise ratio (SNR) in FSK-treated HeLa cells. Plots indicate the SNR of each cell, and red bars are means and SD. For Booster-PKA, 55 cells from a single experiment were used, and for AKAR3EV, 145 cells from a single experiment were used. The p-value was calculated by unpaired two-tailed Welch's t-test.

Similarly, Booster-ERK revealed a gain of 28 ± 3% by EGF stimulation. It is noteworthy that the gains of Booster-JNK, Booster-ROCK, and Booster-ERK were significantly higher than or at least equivalent to the biosensors that were constructed simply by replacing fluorophores of corresponding CFP/YFP-based biosensors (Figure S5). The gains of Booster-JNK and Booster-ERK were smaller than those of CFP/YFP-based ones. On the other hand, the gain of Booster-ROCK was larger than Eevee-ROCK. These results indicate that the Booster backbone provides an easy platform for the development of red-shifted FRET biosensors.

Dual FRET Imaging with Booster. The primary motivation to develop Booster biosensors is to overcome the limitations of dual FRET imaging with CFP/YFP-based FRET biosensors. The excitation and emission spectra of mTurquoise, YPet, mKOκ, and mKate2 and the filter sets used for the multiplexed imaging are illustrated in Figure 4A. With the filter sets shown here, the signal from Turquoise-GL or YPet was separable from the mKOκ and mKate2 signals and vice versa (Figure 4B). For the two-photon imaging, Turquoise-GL and mKOκ were excited at 840 and 1100 nm, respectively. Again, spectral bleedthrough and cross-excitation of the FRET pairs were markedly less than the genuine signals (Figure 4B). As a proof of concept, we coexpressed EKAREV, a CFP/YFP-based FRET biosensor for ERK activity, with Booster-PKA in HeLa cells, and acquired time-lapse images (Figure 4C). During the course of imaging, ERK was stimulated by EGF and inhibited by an MEK inhibitor (PD0325901). PKA was stimulated by a nonselective β-adrenergic agonist, isoproterenol, and inhibited by a β-adrenergic antagonist, propranolol

https://dx.doi.org/10.1021/acssensors.9b01941
ACS Sens. XXXX, XXX, XXX−XXX

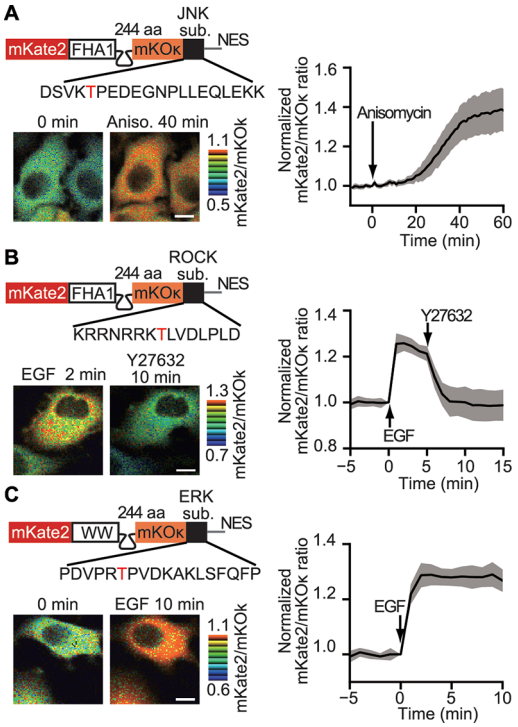

Figure 3. Development of JNK, ROCK, and ERK biosensors based on the Booster backbone. (A) Schematics of Booster-JNK (upper left). Representative IMD images before and 40 min after 1 μg/mL anisomycin stimulation are shown at the lower left; the time course of the emission ratio normalized at time 0 is shown at the right. Results are shown for 17 cells from a single experiment. The solid line represents the means; shaded areas represent SD. (B) Schematics of Booster-ROCK (upper left). Representative IMD images 2 min after 10 ng/mL EGF stimulation and 10 min after 30 μM Y27632 treatment are shown at the lower left; the time course of the emission ratio normalized at time 0 is shown at the right. Results are shown for 20 cells from a single experiment. The solid line represents the means; shaded areas represent SD. (C) Schematics of Booster-ERK (upper left). Representative IMD images before stimulation and 10 min after 10 ng/mL EGF stimulation are shown at the lower left; the time course of the emission ratio normalized at time 0 is shown at the right. Results are shown for 19 cells from a single experiment. The solid line represents the means; shaded areas represent SD. Scale bars, 10 μm.

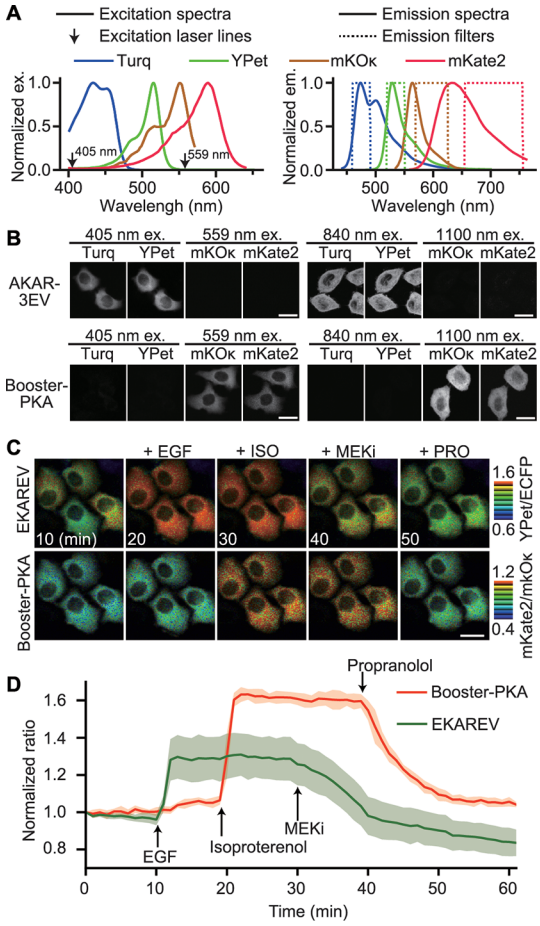

Figure 4. Multiplexed imaging with Booster-PKA. (A) Excitation (left) and emission (right) spectra of Turquoise-GL, YPet, mKOκ, and mKate2 with excitation laser lines (arrows in the left) and emission filters (dashed boxed in the right). (B) HeLa cells expressing AKAR3EV (upper) or Booster-PKA (lower) imaged by confocal microscopy (405 nm ex. and 559 nm ex.) or two-photon excitation microscopy (840 nm ex. and 1100 nm ex.). The excitation wavelengths are shown above. Scale bars, 20 μm. (C) HeLa cells expressing both EKAREV and Booster-PKA time lapse imaged by confocal microscopy. FRET/CFP and mKate2/mKOκ ratios were obtained with a 405 nm laser (104 mW/cm^2, 2.9 s/min) and 559 nm laser (5 mW/cm^2, 2.9 s/min), respectively. During imaging, the following stimulants/inhibitors were added to the cells at the indicated time points, 10 ng/mL EGF, 1 μM isoproterenol (ISO), 1 μM PD0325901 (MEKi), and 10 μM propranolol (PRO), and are shown in the IMD mode. Scale bars, 20 μm. (D) Time courses of the emission ratios normalized at time 0 for EKAREV (green) and Booster-PKA (red) in HeLa cells. Results are shown for six cells from a single experiment. The solid line represents the means; shaded areas represent SD.

(Figure 4D). Although the parental mKOκ and mKate2, mKO and mKate,[36,37] have been reported as photoconvertible with blue or violet light, we concluded that the effect of photoconversion can be negligible at least in our experimental condition. We did not observe any cross-talk between ERK and PKA; both were responsive only to their specific stimulant and inhibitor.

Widening the Dynamic Range for the cAMP Signaling. The activity of the cAMP signaling pathway can be monitored by a number of FRET biosensors;[38] however, each of them does not have a wide dynamic range to cover the physiological dynamic range of cAMP. Biosensors containing the cAMP-binding domain of Epac are generally less sensitive to cAMP than the PKA biosensors.[38,39] By combining Booster-PKA and Epac-based cAMP biosensors, we aimed to quantify a broad range of cAMP signaling activity. First, we developed a hyBRET-Epac biosensor based on a hyBRET backbone[40] and Epac biosensor.[41] The detailed sequence is provided in the Supporting Note. HeLa cells stably expressing both Booster-PKA and hyBRET-Epac were established by a piggyBac transposon system.[42,43] As a proof of concept, we observed the response of biosensors upon gradual increases of forskolin or isoproterenol. The forskolin response of Booster-PKA was observed from 0.2 to 2 μM, and that of hyBRET-Epac was observed from 2 to 50 μM (Figure 5A). Additionally, the isoproterenol response of Booster-PKA was observed from 1 to 10 nM, and that of hyBRET-Epac was observed from 20 to 100 nM. Thus, using the combination of Booster-PKA and hyBRET-Epac, we can monitor the activity change of the cAMP pathway invoked by 0.2−50 μM forskolin and 1−100 nM isoproterenol at the single-cell level.

https://dx.doi.org/10.1021/acssensors.9b01941
ACS Sens. XXXX, XXX, XXX−XXX

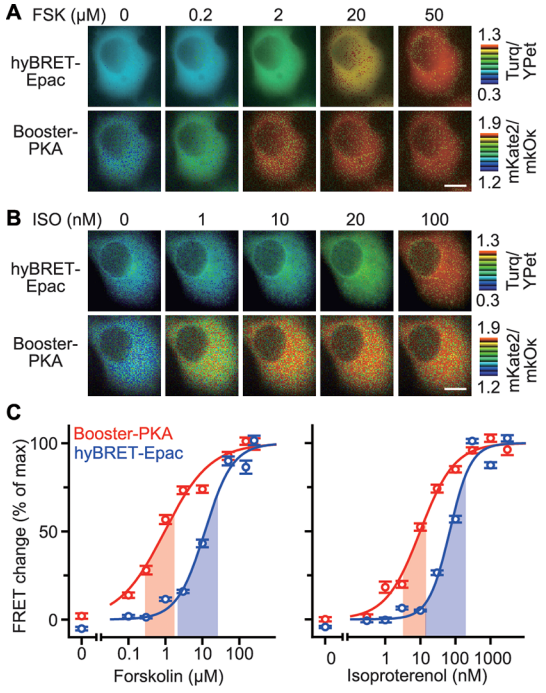

Figure 5. Dynamic ranges for cAMP signaling. (A, B) HeLa cells expressing both hyBRET-Epac and Booster-PKA stimulated with increasing amounts of forskolin (FSK, A) or isoproterenol (ISO, B). Images are shown in the IMD mode. Scale bars, 10 μm. (C) Dose–response curves of hyBRET-Epac and Booster-PKA toward various concentrations of FSK (left) and ISO (right). HeLa cells expressing both hyBRET-Epac and Booster-PKA were plated in a 96-well plate and stimulated with serially diluted forskolin or isoproterenol. FRET ratio images were acquired 10 min after the addition of those drugs. Averaged emission ratios are plotted against the concentrations of FSK or ISO. Data were fitted to the Hill equation. Results are shown for at least 100 cells from one to three experiments. The solid lines represent fitted curves; shaded areas represent the dynamic ranges for the detection; error bars represent 95% confidence intervals.

To examine the response more quantitatively, cells were incubated with serially diluted forskolin or isoproterenol, and the FRET ratios in each cell were quantified and plotted as a function of stimulant concentration (Figure 5C). The dose–response curves were obtained by fitting the data to the Hill equation to determine the minimum and upper limits of detection,[44] which are illustrated with red and blue shaded areas in Figure 5C. The lower and upper limits of detection of forskolin were 0.28 and 1.74 μM, respectively, by using Booster-PKA, and they were 2.1 and 26 μM, respectively, by using hyBRET-Epac. The dynamic range for the detection of forskolin is between 0.28 and 26 μM. Likewise, the dynamic range for the detection of isoproterenol is between 3 and 196 nM. Thus, by using two FRET biosensors simultaneously, we achieved an increase in dynamic range of approximately two orders of magnitude.

Compatibility with bPAC, an Optogenetic Stimulator for PKA. The second motivation for the development of Booster is to overcome the incompatibility of CFP/YFP-based FRET biosensors with blue light-responsive optogenetic tools. To demonstrate that Booster biosensors could overcome this drawback, we employed a *Beggiatoa* photoactivated adenylyl cyclase (bPAC)[7] as an example of the flavoprotein-based optogenetic tools. We coexpressed bPAC and Booster-PKA in HeLa cells (Figure 6A). Illumination of the cells with 430 nm blue light induced PKA activation, as monitored by an increase in the mKate2/mKOκ ratio (Figure 6B).

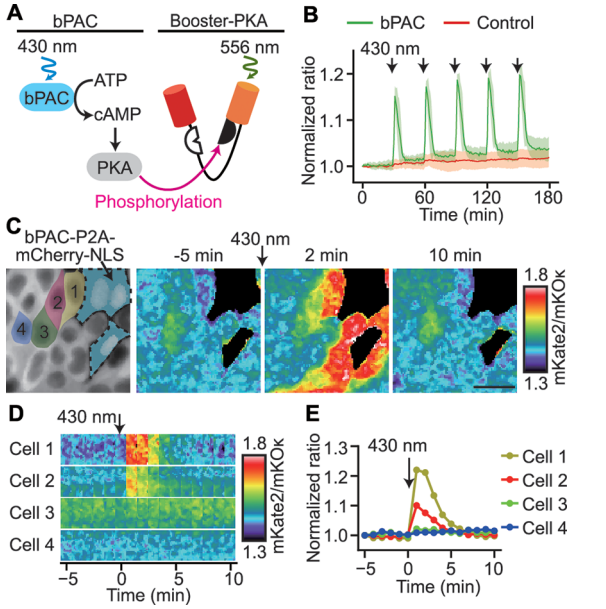

Figure 6. Detection of bPAC-mediated PKA activation. (A) Scheme of the experimental design. (B) bPAC-mediated PKA activation monitored with Booster-PKA. HeLa cells expressing both Booster-PKA and bPAC (green) or expressing Booster-PKA only (red) were imaged with a wide-field fluorescence microscope. The emission ratios of 10 cells are normalized at time 0 and plotted against time. During the course of imaging, cells were illuminated with 9.0 mW cm^{-2}, 430 nm LED every 30 min for 1 s, as indicated by arrows. The solid line represents the means; shaded areas represent SD. (C) Cell-to-cell propagation of the PKA activity. MDCK cells expressing Booster-PKA were cocultured with MDCK cells expressing bPAC-P2A-mCherry-NLS. The left panel shows the fluorescence of mKate2 and mCherry-NLS. Cells expressing bPAC-P2A-mCherry-NLS are marked with a cyan color. The numbers indicate Cell 1 to Cell 4, as denoted in (D). The right three panels show FRET ratio images, wherein the bPAC-expressing cells are masked. Cells were illuminated with 430 nm LED at time 0 for 0.5 s. Scale bar, 20 μm. (D, E) PKA activity in Cell 1 to Cell 4 is shown by montage images (D) and line plots (E).

Previously, cell-to-cell propagation of ERK activity was reported in vitro and in vivo.[45−47] However, it remains unknown whether cAMP activity propagates in monolayers of Madin−Darby canine kidney (MDCK) cells. To explore this idea, we next constructed a polycistronic vector that comprises bPAC and nuclear localized mCherry (mCherry-NLS) connected by self-cleaving P2A peptide sequences.[48] MDCK cells stably expressing bPAC-P2A-mCherry-NLS were cocultured with MDCK cells expressing Booster-PKA at a 1:100 ratio. MDCK cells juxtaposed to the bPAC-expressing cells showed an increase in the mKate2/mKOκ ratio after blue light exposure (Figure 6C−E). Cells that were two cells away from the bPAC-expressing cells, such as Cell 2 in Figure 6D, exhibited a slight increase in the mKate2/mKOκ ratio after blue light exposure. On the other hand, we barely detected an increase in the mKate2/mKOκ ratio in Booster-PKA-expressing MDCK cells located more than two cells away from bPAC-expressing MDCK cells (for example, Cell 3 or Cell 4 in Figure 6D). Although the molecular mechanism of this phenomenon remains to be studied, these results indicate

https://dx.doi.org/10.1021/acssensors.9b01941
ACS Sens. XXXX, XXX, XXX−XXX

that Booster-PKA is compatible with the optogenetic tools that operate at blue light.

Development of Transgenic Mice Expressing Booster-PKA. Finally, to apply Booster-PKA for in vivo microscopy,[49] we generated transgenic mice expressing Booster-PKA by Tol2-mediated gene transfer.[50] The resulting mouse line, which we named lox-Booster-PKAchu, was designed to express mCherry-NLS and Booster-PKA before and after Cre recombination, respectively (Figure 7A). To test the biosensor expression, lox-Booster-PKAchu mice were crossed with EIIa-cre mice, in which Cre is expressed at the zygote stage.[51] We confirmed germ-line transmission of the Booster-PKA gene to the offspring and named the mouse line EIIa-cre/lox-Booster-PKAchu.

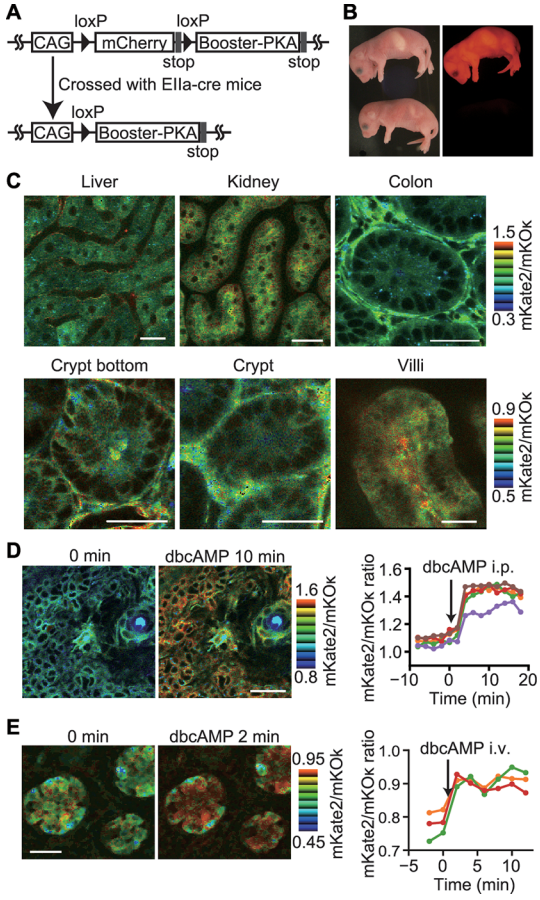

Figure 7. Generation of transgenic mice expressing Booster-PKA. (A) Diagram of the *loxP*-flanked mCherry-NLS cassette upstream of Booster-PKA. (B) Expression of Booster-PKA in a newborn transgenic mouse. An EIIa-cre/lox-Booster-PKAchu mouse (upper) and a control mouse were observed under white light without an emission filter (left) or green light with a red emission filter (right). (C) In vivo imaging of Booster-PKA. An EIIa-cre/lox-Booster-PKAchu mouse was anesthetized and observed under a two-photon microscope with an excitation wavelength of 1040 nm. Representative images are shown in the IMD mode. Top: the liver, the kidney, and the colon. Bottom: the crypt bottom, the crypt, and the villi of the ileum. Scale bars, 30 μm. (D) dbcAMP-induced PKA activation in ear skin cells. Images were obtained before and 10 min after the intraperitoneal injection of 0.3 mg/kg dbcAMP. Shown are FRET ratio images (left) and the time courses of the FRET ratio of five representative cells (right). Scale bar, 30 μm. (E) dbcAMP-induced PKA activation in the crypt of the ileum. Images were obtained before and 2 min after the intravenous injection of 0.3 mg/kg dbcAMP. Ratio images are shown in the IMD mode. Shown are FRET ratio images (left) and the time courses of the FRET ratio of three representative regions (right). Scale bar, 30 μm.

EIIa-cre/lox-Booster-PKAchu mice grew normally and showed no external or internal signs of malformations. The CAG promoter-driven expression of Booster-PKA was sufficiently robust to identify newborn transgenic mice by visual inspection of orange fluorescence in the skin (Figure 7B). The expressed biosensor could be readily imaged in the kidney, liver, colon, and ileum by TPEM (Figure 7C).

To confirm the functional expression of Booster-PKA, the basal layer of the auricular epidermis and the crypt of the ileum were observed under TPEM. Activation of PKA was then induced by intraperitoneal or intravenous injection of dbcAMP, a cell-permeable analog of cAMP. The mKate2/mKOκ ratio increased rapidly after dbcAMP injection (Figure 7D,E), indicating that Booster-PKA detected the PKA activation in vivo. Thus, Booster is a powerful tool for monitoring spatiotemporal biochemical activities in living mice.

DISCUSSION

To the best of our knowledge, most of the previously developed red-shifted FRET pairs failed to surpass the CFP/YFP pair as a backbone for FRET biosensors.[4,52] However, the performance of mKOκ/mKate2-based Booster-PKA is comparable with that of the CFP/YFP-based FRET biosensor AKAR3EV (Figure 2). Moreover, the Booster backbone can be used for the development of other biosensors for protein kinases, ERK, ROCK, and JNK (Figure 3), opening a new window for dual FRET imaging.

The successful development of Booster is largely dependent on the novel order, from the N-terminus, of four components of the FRET biosensor: the acceptor FP, ligand domain (phosphopeptide-binding motif), donor FP, and sensor domain (substrate for protein kinase) (Figure 1B). A FRET biosensor based on the mKO/mKate FRET pair was already developed by Su et al., who used mKOκ and mLumin (mKate-S158A) as the donor and acceptor, respectively.[11,53] The authors used the classical design; that is, the ligand and sensor domains were sandwiched with mKOκ and mLumin. The response of such an mKOκ/mLumin-based biosensor for Src was only marginal. This agrees with our data showing the critical importance of the order of the four components of the FRET biosensor (Figure 1A). Fritz et al. extensively examined the effect of the order of the four components by using teal fluorescence protein (TFP) and YFP as the donor and acceptor, respectively.[54] In this case, FRET biosensors with the prototypal order, in which TFP and YFP sandwich the sensor and ligand domains, overwhelmed the other FRET biosensors. Meanwhile, even in the case of CFP and YFP, the order of these two fluorescent proteins significantly affects the performance of the FRET biosensor.[55] These results indicate that the best order of the four components varies among the different FRET pairs. At the same time, however, the successful development of Booster-ERK, Booster-ROCK, and Booster-JNK by using the same backbone as for Booster-PKA also indicates that Booster's order of the four components can be used to develop more red-shifted FRET biosensors for protein kinases, simply by replacing the substrate and phosphate-binding domains.

Another modification included in Booster is a 244-amino-acid linker. The variation of lifetime after stimulation is larger

https://dx.doi.org/10.1021/acssensors.9b01941
ACS Sens. XXXX, XXX, XXX−XXX

A

		λ (nm)	λex (nm)	εD(λex) (mM^{-1} cm^{-1})	εA(λex) (mM^{-1} cm^{-1})	E (off state)	E (on state)	ϕ_D	$f_D(\lambda)$	ϕ_A	$f_A(\lambda)$
Actual value	Donor ch	564	515	52.5	10.6	0	0.1	0.61	1	variable	0.01
	Acceptor ch	633	515	52.5	10.6	0	0.1	0.61	0.04	variable	1
High bleedthrough	Donor ch	564	515	52.5	10.6	0	0.1	0.61	1	variable	0.5
	Acceptor ch	633	515	52.5	10.6	0	0.1	0.61	0.5	variable	1
Low bleedthrough	Donor ch	564	515	52.5	10.6	0	0.1	0.61	1	variable	0.01
	Acceptor ch	633	515	52.5	10.6	0	0.1	0.61	0.01	variable	1

B

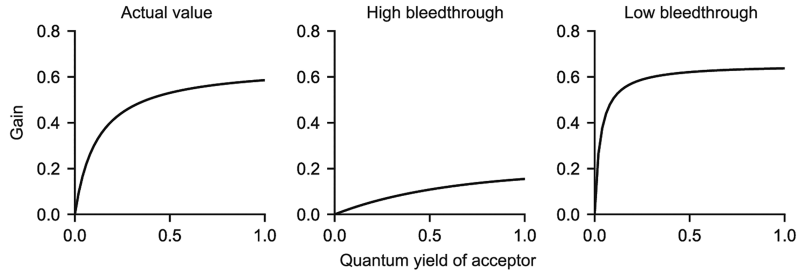

Figure 8. Effect of acceptor QY on the gain of FRET biosensor. (A) Parameters used for the following simulation. (B) Expected gain value when the FRET efficiency changes from 0 (OFF state) to 0.1 (ON state).

with Booster-PKA than with #2 with a 116-amino-acid linker (Figure 1B). Consequently, the improvement of SNR is marginal. We have found a weak negative correlation between the expression level of the biosensor and its lifetime after stimulation in Booster-PKA. Thus, the 244-amino-acid linker might contribute to this large variation. Stable expression of the biosensor may overcome this drawback.

To choose a pair of the fluorescent proteins for the red-shifted FRET biosensor, we first selected the acceptor protein. Although the FRET efficiency is independent of the QY of the acceptor fluorophore, high QY is required for the large sensitized emission of the acceptor.[4,12] We simulated the effect of acceptor QY on the gain of the FRET biosensor the using theoretical fluorescence spectra of the FRET biosensor[40] (see Experimental Section). The estimated gain curves show that QY of the acceptor positively affects the gain even in the low bleedthrough condition (Figure 8). This is the reason why we chose mKate2 for the acceptor despite it having the lowest extinction coefficient among the candidate proteins (Figure S1). As the acceptor, we also used E2-Crimson, the extinction coefficient of which is 2-fold larger than that of mKate2 (Figure S3). Despite the large decrease in the lifetime upon stimulation, the increase in the emission ratio was less than 20% (data not shown), probably due to low QY of E2-Crimson. Thus, the large QY of the acceptor protein is preferable for the detection of sensitized FRET.

Previous studies demonstrated that circular permutants of FPs could be used to greatly improve the dynamic range of FRET biosensors.[54,56] Therefore, use of the circular permutants of mKOκ and mKate2 may improve the dynamic range of Booster. Another well-known method for improving the FRET biosensor is the use of a dimerization-prone FP pair.[30,57−59] However, this approach may not work for the Booster backbone because red-shifted proteins are prone to aggregation.[60]

Fine-tuning of cAMP signaling sometimes plays a critical role in cellular decision-making. For example, Schwann cells proliferate at low concentrations of cAMP analogues or forskolin but differentiate to produce myelin at high concentrations.[61,62] In accordance with this observation, it was reported that PKA-mediated proliferation dominates at low cAMP concentrations, and Epac-mediated myelination dominates at high cAMP concentrations.[63] It has also been reported that low concentrations of cAMP promote but high concentrations of cAMP inhibit the migration of cardiac fibroblasts.[64] These observations prompted us to use the combination of hyBRET-Epac and Booster-PKA for the wide-range quantification of cAMP signaling (Figures 4 and 5). Importantly, the best performance of dual FRET imaging with Booster biosensors and CFP/YFP-based biosensors can be achieved by the optimal choice of excitation wavelength (Figure 4A). We chose a 559 nm laser for the excitation of mKOκ to minimize the excitation of YPet to a negligible level. This excitation slightly decrease the gain compared with 515 nm excitation used in Figure 2 (52 ± 11% versus 79 ± 20%, data not shown). Because mKOκ is 2.5-fold brighter than mKate2 (Figure S1A,B), the cross-excitation of mKate2 does not hamper the ratiometry significantly. However, if the local concentration of the biosensors is very high, then it might be possible that mKOκ quenches YPet through intermolecular FRET.

To date, the transgenic mouse lines expressing Booster-PKA have not exhibited any detectable anomalies or weight loss, and they show the expected Mendelian ratio of hereditary transmission. However, in some tissues, including the pancreas, we have noticed very bright fluorescent protein precipitates. Hirrlinger et al. reported that reef coral fluorescent proteins have a high tendency to form aggregates in transgenic mice in a time-dependent manner.[60] They concluded that the continuous accumulation of proteins leads to precipitation of reef coral fluorescent proteins. It has been reported that the turnover of pancreatic acinar cells takes more than a year.[65] This very slow turnover rate might contribute to the long-term accumulation of biosensor proteins in the pancreas. This problem may be overcome by crossing the Lox-mCherry-Booster-PKAchu with transgenic mice carrying inducible Cre genes such as tetracycline-regulatable systems[66] or tamoxifen-dependent Cre recombinases.[67]

In summary, we have described an optimized backbone for orange and far-red fluorescent protein-based FRET biosensors. The resulting Booster biosensors can be combined with CFP/YFP-based FRET biosensors and a flavoprotein-based optogenetic tool. In addition, the Booster-PKA-expressing

https://dx.doi.org/10.1021/acssensors.9b01941
ACS Sens. XXXX, XXX, XXX−XXX

transgenic mice developed in the present study will accelerate our understanding of spatiotemporal cellular signaling in vivo.

EXPERIMENTAL SECTION

Plasmids. The complementary DNAs (cDNAs) of mKOκ[27] and mKate2[20] were amplified by polymerase chain reaction (PCR). The cDNAs encoding the biosensors were subcloned into the pCAGGS vector[68] using Ligation high Ver. 2 (TOYOBO) or the In-Fusion cloning kit (Clontech). The plasmid encoding bPAC[7] was obtained from Addgene (#28134). Bicistronic vectors expressing bPAC with ECFP-NES and mCherry-NLS were constructed by using a self-cleaving P2A peptide.[48] To construct vectors for the stable expression of biosensor or bPAC-P2A-ECFP-NES in HeLa cells, cDNAs were subcloned into the pPB piggyBac transposon vector.[43] For lentiviral production, cDNAs of Booster-PKA and bPAC-P2A-mCherry-NLS were inserted into the pCSII lentiviral vector.[69] The packaging vector psPAX2 was obtained from Addgene (#12260). The envelope plasmid pCMV-VSV-G-RSV-Rev was a kind gift from Dr. Miyoshi (RIKEN BioResource Center). To generate transgenic mice, we constructed a pT2ADW-lox-mCherry-NLS-Booster-PKA plasmid. The pT2ADW vector was described previously.[40] The DNA encoding mCherry-NLS and the polyA sequence of rabbit beta-globin was amplified by PCR and inserted into the region upstream of Booster-PKA. The DNA sequences of the biosensors are shown in the Supporting Note.

Reagents. Forskolin was purchased from Alomone Labs. EGF, anisomycin, isoproterenol, and propranolol were obtained from Sigma-Aldrich. PD0325901 and Y-27632 were purchased from FUJIFILM Wako Pure Chemical Corporation.

Cell Culture and Establishment of Cell Lines. HeLa cells were purchased from the Human Science Research Resources Bank. HEK-293T cells were obtained from Invitrogen as Lenti-X 293T cells. MDCK cells were purchased from the RIKEN BioResource Center (no. RCB0995). HeLa, HEK-293T, and MDCK cells were maintained in Dulbecco's modified Eagle medium (DMEM; FUJIFILM Wako Pure Chemical Corporation) containing 10% fetal bovine serum (SAFC Biosciences) and 1% penicillin−streptomycin (Nacalai Tesque). To obtain HeLa cells stably expressing both Booster-PKA and bPAC-P2A-ECFP-NES, we utilized a piggyBac transposon system. MDCK cell lines were established with lentivirus-mediated gene transfer. For lentiviral production, HEK-293T cells were cotransfected with the pCSII plasmids, together with psPAX2 and pCMV-VSV-G-RSV-Rev.

Calculation of Förster Distance. Förster distance R_0 (in Å) was calculated using the equation[70]

$$R_0 = 9.78 \times 10^3 (Q_D J n^{-4} \kappa^2)^{1/6}$$

where κ^2 is the orientation factor (the rotationally averaged value of 2/3 was used), n = 1.33 is the refractive index of water, Q_D is the quantum yield of the donor, and J is the spectral overlap integral calculated as

$$J = \frac{\int f_D(\lambda)\varepsilon_A(\lambda)\lambda^4 \, d\lambda}{\int f_D(\lambda) d\lambda}$$

where λ is the wavelength, f_D is the un-normalized donor emission spectrum, and ε_A is the acceptor molar extinction coefficient.

Fluorescence Lifetime Imaging Microscopy (FLIM). HeLa cells were plated on 35 mm glass-base dishes (AGC Inc.) coated with collagen type I (Nitta Gelatin). The plasmid-encoding biosensors were transfected with 293fectin (Thermo Fisher Scientific). After 24−48 h, the cells were serum-starved for at least 3 h with DMEM/F12 supplemented with 0.1% bovine serum albumin (BSA; Sigma-Aldrich). Two-photon (2P) FLIM was performed with an FV1000MPE inverted microscope equipped with a 30×/1.05 NA silicon oil-immersion objective lens (UPLSAPO 30XS; Olympus), a Mai Tai DeepSee Ti:Sapphire laser (Spectra-Physics), an IR-cut filter, RDM690 (Olympus), and an emission filter, BA510-550 (Olympus). The excitation wavelength was tuned to 1000 nm. The fluorescence lifetime images were obtained using a time-correlated single-photon counting mode (SPC-150; Becker and Hickl) and processed by SPC Image software (Becker and Hickl) according to the manufacturer's protocol.

Confocal and Two-Photon Fluorescence Imaging of Cultured Cells. HeLa cells were plated on 24-well glass-bottom plates (AGC Inc.) coated with collagen type I. The plasmid-encoding biosensors were transfected with 293fectin. After 24−48 h, the cells were serum-starved for at least 3 h with DMEM/F12 supplemented with 0.1% BSA.

Confocal fluorescence images were acquired using an IX81 inverted microscope (Olympus) equipped with an FV1000 confocal imaging system (Olympus) and a 20×/0.75 NA dry objective lens (UPLSAPO 20X; Olympus) under the following sets of conditions. For CFP and FRET imaging, we used a 440 nm excitation laser, DM 405−440/515 dichroic mirror, and 460−490 nm and 520−550 nm for CFP and YFP, respectively. For mKOκ and mKate2 imaging, we used a 515 nm excitation laser, DM 405-440/515 dichroic mirror, and 545−575 nm and 655−755 nm for mKOκ and mKate2, respectively. For multiplexed FRET imaging, we used a 405 nm excitation laser for CFP and YFP, 559 nm excitation laser for mKOκ and mKate2, DM 405/488/559 dichroic mirror, and 460−490, 520−550, 570−625, and 655−755 nm for CFP, YFP, mKOκ, and mKate2, respectively.

Two-photon images were acquired with an FV1200MPE-IX83 inverted microscope (Olympus) equipped with a 30×/1.05 NA silicon oil-immersion objective lens (UPLSAPO 30XS; Olympus), an InSight DeepSee Ultrafast laser (Spectra-Physics), and an IR-cut filter, RDM690 (Olympus). The optical filters used for the imaging were as follows: three dichroic mirrors; T515lpxru, T565spxr, and T610lpxr (Chroma Technology Corp.); and four emission filters, ET480/40m for CFP, AT545/30m for YFP, ET590/40m for mKOκ, and ET645/75m for mKate2. The excitation wavelengths were 840 and 1100 nm for CFP and mKOκ, respectively.

The summary of filter sets is described in the Supporting Note.

Wide-Field Fluorescence Microscopy and Quantification of Drug Response. For wide-field microscopy, cells were imaged with an IX83 inverted microscope (Olympus) equipped with an UPLSAPO 10X or 20X objective (Olympus), a Prime sCMOS camera (Photometrics), a CoolLED precisExcite light-emitting diode (LED) illumination system (Molecular Devices), an IX2-ZDC laser-based autofocusing system (Olympus), and an MD-XY30100T-Meta automatically programmable XY stage (SIGMA KOKI). The following filters were used for the multiplexed imaging: for CFP and YFP imaging, an ET430/24x (Chroma Technology Corp.) excitation filter, XF2034 (455DRLP) (Omega Optical) dichroic mirror, and FF01-483/32 (Semrock) and ET535-30m (Chroma Technology Corp.) for CFP and YFP, respectively; for mKOκ and mKate2 imaging, an FF01-556/20 (Semrock) excitation filter, FF562-Di03 (Semrock) dichroic mirror, and XF3024 (590DF35) (Omega Optical) and ET632/60m (Chroma Technology Corp.) for mKOκ and mKate2, respectively.

Images were processed and analyzed with MetaMorph software, as described previously.[71] Briefly, the FRET efficiency was visualized as YFP/CFP, CFP/YFP, or mKate2/mKOκ ratio images shown in the intensity-modulated display mode (IMD), in which eight colors from red to blue represent each ratio and the 32 grades of color intensity represent the fluorescence intensity of each acceptor fluorophore according to the color scale shown in each figure.

For visualization of the response of Booster-PKA and hyBRET-Epac to a wide range of stimulation, we first established HeLa cells expressing both Booster-PKA and hyBRET-Epac. Cells were plated on 35 mm glass-base dishes (AGC Inc.) coated with collagen type I. After 24 h, the cells were serum-starved for 3−6 h with DMEM/F12 supplemented with 0.1% BSA (Sigma-Aldrich). Fluorescence images were acquired with an UPLSAPO 40X objective (Olympus). The forskolin and isoproterenol concentrations were gradually increased from 10 nM to 50 μM and from 0.1 nM to 1 μM, respectively.

For the determination of the dynamic range for the drug response, HeLa cells expressing both Booster-PKA and hyBRET-Epac were plated into 96-well glass-bottom dishes and stimulated with serially

https://dx.doi.org/10.1021/acssensors.9b01941
ACS Sens. XXXX, XXX, XXX−XXX

diluted forskolin or isoproterenol. Ten minutes after stimulation, fluorescence images were acquired with an UPLSAPO 10X objective. Cells were identified by autothreshold, and the fluorescence intensities in each region of interest were quantified and used in the following analysis. First, the Turquoise-GL/YPet and mKate2/mKOκ ratios were quantified in each cell. From the dataset at each time point, the interquartile range (IQR) was calculated to exclude the outliers by using 1.5*IQR as the limit. Using this data set, the mean (μ) and standard deviation (σ) were calculated at each time point. Then, the Turquoise-GL/YPet or mKate2/mKOκ ratios versus concentrations of forskolin or isoproterenol were fitted to the Hill equation to obtain the dose-responsive function f(concentration). The minimum and maximum limits of detection were defined as follows

$$f(\text{minimum limit of detection}) = \mu_0 + 2\sigma_0$$

$$f(\text{maximum limit of detection}) = \mu_{max} - 2\sigma_{max}$$

where μ_0 and σ_0 are the average and standard deviation in the absence of reagents, and μ_{max} and σ_{max} are the average and standard deviation at the highest concentration of reagents, respectively.

Spectroscopy. For the measurement of single-photon-excited fluorescence spectra, cells were observed with an inverted microscope (IX81; Olympus) equipped with a 60×/1.4 oil-immersion objective lens (PlanApo PH3; Olympus). CFP was excited by an FF02-438/24 (Semrock) excitation filter and an FF458-Di02-25x36 (Semrock) dichroic mirror. mKOκ was excited by a 470F2 (Asahi Spectra) and a DM500 (Olympus) dichroic mirror. The fluorescence spectra were recorded with a PMA-12 photonic multichannel analyzer (Hamamatsu Photonics).

For the measurement of two-photon-excited fluorescence spectra, cells were observed with an upright microscope (SP8 FALCON; Leica) equipped with a 25×/1.0 NA water-immersion objective lens (HC IRAPO L; Leica). The two-photon-excited fluorescence spectra were acquired in lambda scanning mode upon excitation of CFP at a wavelength of 840 nm and mKOκ at a wavelength of 1000 nm.

Optogenetic Experiments with bPAC. HeLa cells transiently expressing both bPAC-P2A-ECFP-NES and Booster-PKA or expressing Booster-PKA only were plated on 24-well glass-bottom plates (AGC Inc.) coated with collagen type I. One day after seeding, the cells were serum-starved for at least 3 h with DMEM/F12 supplemented with 0.1% BSA (Sigma-Aldrich). MDCK cells stably expressing bPAC-P2A-mCherry-NLS or Booster-PKA were mixed at a 1:100 ratio and plated on 96-well glass-bottom plates (AGC Inc.). One day after seeding, the medium was replaced with phenol red-free M199 (Invitrogen) supplemented with 10% fetal bovine serum. Cells were imaged by wide-field fluorescence microscopy, as described above. bPAC was activated with excitation light for CFP imaging.

Transgenic Mice. To generate EIIa-cre mice, we crossed B6.FVB-Tg (EIIa-cre)C5379Lmgd/J mice (a gift from Mitinori Saitou, Kyoto University, Kyoto, Japan) with B6N-Tyrc-Brd/BrdCrCrl mice, also known as B6 Albino mice (Japan SLC), for more than 10 generations. Offspring were routinely genotyped by PCR with primers 5′-ATTTGCCTGCATTACCGGTC-3′ and 5′-ATCAACGTTTTCTTTTCGG-3′. Transgenic mice expressing Booster-PKA were generated by Tol2-mediated gene transfer, as previously described.[72] Briefly, fertilized eggs derived from C57BL/6N mice were microinjected with a mixture of Tol2 transposase mRNA and pT2ADW-lox-mCherry-NLS-Booster-PKA plasmid. Transgenic male mice were crossed with female EIIa-cre mice for the ubiquitous expression of Booster-PKA.

Newborn mice were illuminated with a green LED and inspected for red fluorescence through a red filter, LED530-3WRF (Optocode). Mice were housed in a specific pathogen-free facility and received a routine chow diet and water ad libitum. To date, no disease or anomaly has been associated with the transgenic mice used in this study. Male and female mice of 4−40 weeks of age were used for the in vivo imaging. At the end of the experiments, euthanasia was performed by anesthetic overdose. The animal protocols were reviewed and approved by the Animal Care and Use Committee of Kyoto University Graduate School of Medicine (nos. 10584, 14079, 15064, 16038, and 17539), and the methods were carried out in accordance with the relevant guidelines and regulations.

In Vivo Two-Photon Imaging of Mouse Epidermis. Mice were anesthetized with 1.5% isoflurane (FUJIFILM Wako Pure Chemical Corp.) inhalation and placed in the supine position on an electric heat pad maintained at 37 °C. Depilation cream was used to remove the hair of mice before the experiments. For observations of the liver, kidney, colon, and ileum, a small vertical incision was made in the abdominal wall to expose the tissues. The exposed tissues and ear skin were immobilized on a custom-made vacuum-stabilized imaging window (Olympus), as described previously.[73] The suction force was set to approximately 30 kPa. The vacuum-stabilized imaging window was kept to 37 °C with a lens heater (TP-LH; Tokai Hit).

2P excitation microscopy was performed with an FV1200MPE-BX61WI upright microscope (Olympus) equipped with a 25×/1.05 water-immersion objective lens (XLPLN 25XWMP; Olympus), an InSight DeepSee Ultrafast laser, an IR-cut filter (BA685RIF-3), two dichroic mirrors, DM505 (Olympus) and T610lpxr, and two emission filters FF01-579/34 (Semrock) and ET645/75m for mKOκ and mKate2, respectively. The excitation wavelength for mKOκ was 1040 nm.

Theoretical Fluorescence Spectra of the FRET Biosensor. The theoretical fluorescence spectra are described by the following equation.[40]

$$F(\lambda) = \varepsilon_D(\lambda_{ex})\{(1-E)\times\phi_D\times f_D(\lambda) + E\times\phi_A\times f_A(\lambda)\} + \varepsilon_A(\lambda_{ex})\times\phi_A\times f_A(\lambda) \quad (1)$$

where $F(\lambda)$ is the fluorescence at wavelength λ, $\varepsilon_D(\lambda_{ex})$ is the excitation coefficient of the donor at the excitation wavelength, E is the FRET efficiency between the donor and the acceptor, ϕ_D is the quantum yield of the donor, $f_D(\lambda)$ is the normalized emission of the donor at wavelength λ, ϕ_A is the quantum yield of the acceptor, $f_A(\lambda)$ is the normalized emission of the acceptor, and $\varepsilon_A(\lambda_{ex})$ is the extinction coefficient of the acceptor at the excitation wavelength. From this equation, we can estimate the effect of acceptor QY on the gain of biosensor.

Statistical Analysis. All statistical analyses were performed using Excel software (Microsoft). No statistical analysis was used to predetermine the sample size. Welch's t-test was used to evaluate statistically significant differences. The p-values less than 0.05 were considered statistically significant.

■ ASSOCIATED CONTENT

Supporting Information

The Supporting Information is available free of charge at https://pubs.acs.org/doi/10.1021/acssensors.9b01941.

Properties of fluorescent proteins; optimization of the order of components; mScarlet/E2-Crimson-based FRET biosensor; application of the arrangement of Booster to the CFP/YFP pair; application of the Booster backbone for the biosensors of JNK, ROCK, and ERK; and nucleotide sequences of biosensors (PDF)

■ AUTHOR INFORMATION

Corresponding Author

Kenta Terai − *Research Center for Dynamic Living Systems, Graduate School of Biostudies, Kyoto University, Kyoto 606-8501, Japan*; Email: terai.kenta.5m@kyoto-u.ac.jp

Authors

Tetsuya Watabe − *Department of Pathology and Biology of Diseases, Graduate School of Medicine, Kyoto University, Kyoto 606-8501, Japan*; orcid.org/0000-0002-9561-9679

https://dx.doi.org/10.1021/acssensors.9b01941
ACS Sens. XXXX, XXX, XXX−XXX

Kenta Sumiyama − *Laboratory for Mouse Genetic Engineering, RIKEN Center for Biosystems Dynamics Research, Osaka 565-0874, Japan*

Michiyuki Matsuda − *Department of Pathology and Biology of Diseases, Graduate School of Medicine and Research Center for Dynamic Living Systems, Graduate School of Biostudies, Kyoto University, Kyoto 606-8501, Japan*

Complete contact information is available at: https://pubs.acs.org/10.1021/acssensors.9b01941

Author Contributions

T.W., K.T., and M.M. designed the experiments. T.W. performed most of the experiments. K.S. generated transgenic mice. T.W., K.T., and M.M. analyzed the data and wrote the manuscript.

Notes

The authors declare no competing financial interest.

■ ACKNOWLEDGMENTS

We thank the members of the Matsuda Laboratory for their helpful input and encouragement, K. Hirano and K. Takakura for their technical assistance, and the Medical Research Support Center of Kyoto University for in vivo imaging. We also thank S. Osari (Leica) for the technical assistance. Financial support for this article was provided in the form of JSPS KAKENHI18K07066 (K.T.), JSPS KAKENHI19H00993, JSPS KAKENHI15H05949 "Resonance Bio", JSPS KAKENHI16H06280 "ABiS", and CRESTJPMJCR1654 (M.M.) grants and the Fellowship from Takeda Science Foundation (T.W.).

■ REFERENCES

(1) Jares-Erijman, E. A.; Jovin, T. M. FRET imaging. *Nat. Biotechnol.* **2003**, *21*, 1387.

(2) Greenwald, E. C.; Mehta, S.; Zhang, J. Genetically Encoded Fluorescent Biosensors Illuminate the Spatiotemporal Regulation of Signaling Networks. *Chem. Rev.* **2018**, *118*, 11707−11794.

(3) Terai, K.; Imanishi, A.; Li, C.; Matsuda, M. Two decades of genetically encoded biosensors based on Förster resonance energy transfer. *Cell Struct. Funct.* **2019**, *44*, 153.

(4) Bajar, B. T.; Wang, E. S.; Zhang, S.; Lin, M. Z.; Chu, J. A Guide to Fluorescent Protein FRET Pairs. *Sensors* **2016**, *16*, 1488.

(5) Kennedy, M. J.; Hughes, R. M.; Peteya, L. A.; Schwartz, J. W.; Ehlers, M. D.; Tucker, C. L. Rapid blue-light−mediated induction of protein interactions in living cells. *Nat. Methods* **2010**, *7*, 973.

(6) Wu, Y. I.; Frey, D.; Lungu, O. I.; Jaehrig, A.; Schlichting, I.; Kuhlman, B.; Hahn, K. M. A genetically encoded photoactivatable Rac controls the motility of living cells. *Nature* **2009**, *461*, 104.

(7) Stierl, M.; Stumpf, P.; Udwari, D.; Gueta, R.; Hagedorn, R.; Losi, A.; Gärtner, W.; Petereit, L.; Efetova, M.; Schwarzel, M.; et al. Light Modulation of Cellular cAMP by a Small Bacterial Photoactivated Adenylyl Cyclase, bPAC, of the Soil Bacterium Beggiatoa. *J. Biol. Chem.* **2011**, *286*, 1181−1188.

(8) Ouyang, M.; Huang, H.; Shaner, N. C.; Remacle, A. G.; Shiryaev, S. A.; Strongin, A. Y.; Tsien, R. Y.; Wang, Y. Simultaneous Visualization of Protumorigenic Src and MT1-MMP Activities with Fluorescence Resonance Energy Transfer. *Cancer Res.* **2010**, *70*, 2204−2212.

(9) Miranda, J. G.; Weaver, A. L.; Qin, Y.; Park, J. G.; Stoddard, C. I.; Lin, M. Z.; Palmer, A. E. New Alternately Colored FRET Sensors for Simultaneous Monitoring of Zn2+ in Multiple Cellular Locations. *PLoS One* **2012**, *7*, No. e49371.

(10) Lindenburg, L. H.; Hessels, A. M.; Ebberink, E. H. T. M.; Arts, R.; Merkx, M. Robust Red FRET Sensors Using Self-Associating Fluorescent Domains. *ACS Chem. Biol.* **2013**, *8*, 2133−2139.

(11) Su, T.; Zhang, Z.; Luo, Q. Ratiometric fluorescence imaging of dual bio-molecular events in single living cells using a new FRET pair mVenus/mKOκ-based biosensor and a single fluorescent protein biosensor. *Biosens. Bioelectron.* **2012**, *31*, 292−298.

(12) Carlson, H. J.; Campbell, R. E. Genetically encoded FRET-based biosensors for multiparameter fluorescence imaging. *Curr. Opin. Biotechnol.* **2009**, *20*, 19−27.

(13) Zlobovskaya, O. A.; Sergeeva, T. F.; Shirmanova, M. V.; Dudenkova, V. V.; Sharonov, G. V.; Zagaynova, E. V.; Lukyanov, K. A. Genetically encoded far-red fluorescent sensors for caspase-3 activity. *BioTechniques* **2016**, *60*, 62.

(14) Shcherbakova, D. M.; Cox Cammer, N.; Huisman, T. M.; Verkhusha, V. V.; Hodgson, L. Direct multiplex imaging and optogenetics of Rho GTPases enabled by near-infrared FRET. *Nat. Chem. Biol* **2018**, *14*, 591−600.

(15) Oliinyk, O. S.; Shemetov, A. A.; Pletnev, S.; Shcherbakova, D. M.; Verkhusha, V. V. Smallest near-infrared fluorescent protein evolved from cyanobacteriochrome as versatile tag for spectral multiplexing. *Nat. Commun.* **2019**, *10*, 279.

(16) Shcherbakova, D. M.; Stepanenko, O. V.; Turoverov, K. K.; Verkhusha, V. V. Near-Infrared Fluorescent Proteins: Multiplexing and Optogenetics across Scales. *Trends Biotechnol.* **2018**, *36*, 1230−1243.

(17) Ai, H.; Hazelwood, K. L.; Davidson, M. W.; Campbell, R. E. Fluorescent protein FRET pairs for ratiometric imaging of dual biosensors. *Nat. Methods* **2008**, *5*, 401.

(18) Niino, Y.; Hotta, K.; Oka, K. Simultaneous Live Cell Imaging Using Dual FRET Sensors with a Single Excitation Light. *PLoS One* **2009**, *4*, No. e6036.

(19) Grant, D. M.; Zhang, W.; McGhee, E. J.; Bunney, T. D.; Talbot, C. B.; Kumar, S.; Munro, I.; Dunsby, C.; Neil, M. A. A.; Katan, M.; et al. Multiplexed FRET to Image Multiple Signaling Events in Live Cells. *Biophys. J.* **2008**, *95*, L69−L71.

(20) Shcherbo, D.; Murphy, C. S.; Ermakova, G. V.; Solovieva, E. A.; Chepurnykh, T. V.; Shcheglov, A. S.; Verkhusha, V. V.; Pletnev, V. Z.; Hazelwood, K. L.; Roche, P. M.; et al. Far-red fluorescent tags for protein imaging in living tissues. *Biochem. J.* **2009**, *418*, 567−574.

(21) Chu, J.; Haynes, R. D.; Corbel, S. Y.; Li, P.; González-González, E.; Burg, J. S.; Ataie, N. J.; Lam, A. J.; Cranfill, P. J.; Baird, M. A.; et al. Non-invasive intravital imaging of cellular differentiation with a bright red-excitable fluorescent protein. *Nat. Methods* **2014**, *11*, 572.

(22) Bajar, B. T.; Lam, A. J.; Badiee, R. K.; Oh, Y.-H.; Chu, J.; Zhou, X. X.; Kim, N.; Kim, B. B.; Chung, M.; Yablonovitch, A. L.; et al. Fluorescent indicators for simultaneous reporting of all four cell cycle phases. *Nat. Methods* **2016**, *13*, 993−996.

(23) Strack, R. L.; Hein, B.; Bhattacharyya, D.; Hell, S. W.; Keenan, R. J.; Glick, B. S. A Rapidly Maturing Far-Red Derivative of DsRed-Express2 for Whole-Cell Labeling†. *Biochemistry* **2009**, *48*, 8279−8281.

(24) Goedhart, J.; von Stetten, D.; Noirclerc-Savoye, M.; Lelimousin, M.; Joosen, L.; Hink, M. A.; van Weeren, L.; Gadella, T. W. J., Jr.; Royant, A. Structure-guided evolution of cyan fluorescent proteins towards a quantum yield of 93%. *Nat. Commun* **2012**, *3*, 751.

(25) Shaner, N. C.; Lambert, G. G.; Chammas, A.; Ni, Y.; Cranfill, P. J.; Baird, M. A.; Sell, B. R.; Allen, J. R.; Day, R. N.; Israelsson, M.; et al. A bright monomeric green fluorescent protein derived from Branchiostoma lanceolatum. *Nat. Methods* **2013**, *10*, 407.

(26) Kremers, G.-J.; Goedhart, J.; van Munster, E. B.; Gadella, T. W. J. Cyan and Yellow Super Fluorescent Proteins with Improved Brightness, Protein Folding, and FRET Förster Radius. *Biochemistry* **2006**, *45*, 6570−6580.

(27) Tsutsui, H.; Karasawa, S.; Okamura, Y.; Miyawaki, A. Improving membrane voltage measurements using FRET with new fluorescent proteins. *Nat. Methods* **2008**, *5*, 683.

(28) Bindels, D. S.; Haarbosch, L.; van Weeren, L.; Postma, M.; Wiese, K. E.; Mastop, M.; Aumonier, S.; Gotthard, G.; Royant, A.; Hink, M. A.; et al. mScarlet: a bright monomeric red fluorescent protein for cellular imaging. *Nat. Methods* **2016**, *14*, 53.

(29) Shaner, N. C.; Campbell, R. E.; Steinbach, P. A.; Giepmans, B. N. G.; Palmer, A. E.; Tsien, R. Y. Improved monomeric red, orange and yellow fluorescent proteins derived from Discosoma sp. red fluorescent protein. *Nat. Biotechnol.* **2004**, *22*, 1567−1572.
(30) Komatsu, N.; Aoki, K.; Yamada, M.; Yukinaga, H.; Fujita, Y.; Kamioka, Y.; Matsuda, M. Development of an optimized backbone of FRET biosensors for kinases and GTPases. *Mol. Biol. Cell* **2011**, *22*, 4647−4656.
(31) Goedhart, J.; van Weeren, L.; Hink, M. A.; Vischer, N. O. E.; Jalink, K.; Gadella, T. W. J., Jr. Bright cyan fluorescent protein variants identified by fluorescence lifetime screening. *Nat. Methods* **2010**, *7*, 137.
(32) Nguyen, A. W.; Daugherty, P. S. Evolutionary optimization of fluorescent proteins for intracellular FRET. *Nat. Biotechnol.* **2005**, *23*, 355−360.
(33) Fosbrink, M.; Aye-Han, N.-N.; Cheong, R.; Levchenko, A.; Zhang, J. Visualization of JNK activity dynamics with a genetically encoded fluorescent biosensor. *Proc. Natl. Acad. Sci.* **2010**, *107*, 5459−5464.
(34) Li, C.; Imanishi, A.; Komatsu, N.; Terai, K.; Amano, M.; Kaibuchi, K.; Matsuda, M. A FRET biosensor for ROCK based on a consensus substrate sequence identified by KISS technology. *Cell Struct. Funct.* **2017**, *42*, 1−13.
(35) Harvey, C. D.; Ehrhardt, A. G.; Cellurale, C.; Zhong, H.; Yasuda, R.; Davis, R. J.; Svoboda, K. A genetically encoded fluorescent sensor of ERK activity. *Proc. Natl. Acad. Sci.* **2008**, *105*, 19264−19269.
(36) Kremers, G.-J.; Hazelwood, K. L.; Murphy, C. S.; Davidson, M. W.; Piston, D. W. Photoconversion in orange and red fluorescent proteins. *Nat. Methods* **2009**, *6*, 355−358.
(37) Goedhart, J.; Vermeer, J. E. M.; Adjobo-Hermans, M. J. W.; van Weeren, L.; Gadella, T. W. J. Sensitive Detection of p65 Homodimers Using Red-Shifted and Fluorescent Protein-Based FRET Couples. *PLoS One* **2007**, *2*, No. e1011.
(38) Koschinski, A.; Zaccolo, M. Activation of PKA in cell requires higher concentration of cAMP than in vitro: implications for compartmentalization of cAMP signalling. *Sci. Rep.* **2017**, *7*, 14090.
(39) Castro, L. R. V.; Gervasi, N.; Guiot, E.; Cavellini, L.; Nikolaev, V. O.; Paupardin-Tritsch, D.; Vincent, P. Type 4 Phosphodiesterase Plays Different Integrating Roles in Different Cellular Domains in Pyramidal Cortical Neurons. *J. Neurosci.* **2010**, *30*, 6143−6151.
(40) Komatsu, N.; Terai, K.; Imanishi, A.; Kamioka, Y.; Sumiyama, K.; Jin, T.; Okada, Y.; Nagai, T.; Matsuda, M. A platform of BRET-FRET hybrid biosensors for optogenetics, chemical screening, and in vivo imaging. *Sci. Rep.* **2018**, *8*, 8984.
(41) Ponsioen, B.; Zhao, J.; Riedl, J.; Zwartkruis, F.; van der Krogt, G.; Zaccolo, M.; Moolenaar, W. H.; Bos, J. L.; Jalink, K. Detecting cAMP-induced Epac activation by fluorescence resonance energy transfer: Epac as a novel cAMP indicator. *EMBO Rep.* **2004**, *5*, 1176−1180.
(42) Aoki, K.; Komatsu, N.; Hirata, E.; Kamioka, Y.; Matsuda, M. Stable expression of FRET biosensors: A new light in cancer research. *Cancer Sci.* **2012**, *103*, 614−619.
(43) Yusa, K.; Rad, R.; Takeda, J.; Bradley, A. Generation of transgene-free induced pluripotent mouse stem cells by the piggyBac transposon. *Nat. Methods* **2009**, *6*, 363.
(44) Long, G. L.; Winefordner, J. D. Limit of Detection A Closer Look at the IUPAC Definition. *Anal. Chem.* **1983**, *55*, 712A−724A.
(45) Aoki, K.; Kumagai, Y.; Sakurai, A.; Komatsu, N.; Fujita, Y.; Shionyu, C.; Matsuda, M. Stochastic ERK Activation Induced by Noise and Cell-to-Cell Propagation Regulates Cell Density-Dependent Proliferation. *Mol. Cell* **2013**, *52*, 529−540.
(46) Hiratsuka, T.; Fujita, Y.; Naoki, H.; Aoki, K.; Kamioka, Y.; Matsuda, M. Intercellular propagation of extracellular signal-regulated kinase activation revealed by in vivo imaging of mouse skin. *Elife* **2015**, *4*, No. e05178.
(47) Aoki, K.; Kondo, Y.; Naoki, H.; Hiratsuka, T.; Itoh, R. E.; Matsuda, M. Propagating Wave of ERK Activation Orients Collective Cell Migration. *Dev. Cell* **2017**, *43*, 305−317.e5.
(48) Lo, C.-A.; Kays, I.; Emran, F.; Lin, T.-J.; Cvetkovska, V.; Chen, B. E. Quantification of Protein Levels in Single Living Cells. *Cell Rep.* **2015**, *13*, 2634−2644.
(49) Nobis, M.; Warren, S. C.; Lucas, M. C.; Murphy, K. J.; Herrmann, D.; Timpson, P. Molecular mobility and activity in an intravital imaging setting - Implications for cancer progression and targeting. *J. Cell Sci.* **2018**, *131*, jcs206995.
(50) Kamioka, Y.; Sumiyama, K.; Mizuno, R.; Sakai, Y.; Hirata, E.; Kiyokawa, E.; Matsuda, M. Live Imaging of Protein Kinase Activities in Transgenic Mice Expressing FRET Biosensors. *Cell Struct. Funct.* **2012**, *37*, 65−73.
(51) Lakso, M.; Pichel, J. G.; Gorman, J. R.; Sauer, B.; Okamoto, Y.; Lee, E.; Alt, F. W.; Westphal, H. Efficient in vivo manipulation of mouse genomic sequences at the zygote stage. *Proc. Natl. Acad. Sci.* **1996**, *93*, 5860−5865.
(52) Sanford, L.; Palmer, A. Chapter One - Recent Advances in Development of Genetically Encoded Fluorescent Sensors. *Methods Enzymol.* **2017**, *589*, 1−49.
(53) Chu, J.; Zhang, Z.; Zheng, Y.; Yang, J.; Qin, L.; Lu, J.; Huang, Z.-L.; Zeng, S.; Luo, Q. A novel far-red bimolecular fluorescence complementation system that allows for efficient visualization of protein interactions under physiological conditions. *Biosens. Bioelectron.* **2009**, *25*, 234−239.
(54) Fritz, R. D.; Letzelter, M.; Reimann, A.; Martin, K.; Fusco, L.; Ritsma, L.; Ponsioen, B.; Fluri, E.; Schulte-Merker, S.; van Rheenen, J.; et al. A Versatile Toolkit to Produce Sensitive FRET Biosensors to Visualize Signaling in Time and Space. *Sci. Signal.* **2013**, *6*, rs12−rs12.
(55) Ohta, Y.; Kamagata, T.; Mukai, A.; Takada, S.; Nagai, T.; Horikawa, K. Nontrivial Effect of the Color-Exchange of a Donor/Acceptor Pair in the Engineering of Förster Resonance Energy Transfer (FRET)-Based Indicators. *ACS Chem. Biol.* **2016**, *11*, 1816−1822.
(56) Nagai, T.; Yamada, S.; Tominaga, T.; Ichikawa, M.; Miyawaki, A. Expanded dynamic range of fluorescent indicators for Ca2+ by circularly permuted yellow fluorescent proteins. *Proc. Natl. Acad. Sci. U. S. A.* **2004**, *101*, 10554−10559.
(57) Ohashi, T.; Galiacy, S. D.; Briscoe, G.; Erickson, H. P. An experimental study of GFP-based FRET, with application to intrinsically unstructured proteins. *Protein Sci.* **2007**, *16*, 1429−1438.
(58) Kotera, I.; Iwasaki, T.; Imamura, H.; Noji, H.; Nagai, T. Reversible dimerization of aequorea victoria fluorescent proteins increases the dynamic range of FRET-based indicators. *ACS Chem. Biol.* **2010**, *5*, 215−222.
(59) Tang, S.; Yasuda, R. Imaging ERK and PKA Activation in Single Dendritic Spines during Structural Plasticity. *Neuron* **2017**, *93*, 1315.
(60) Hirrlinger, P. G.; Scheller, A.; Braun, C.; Quintela-Schneider, M.; Fuss, B.; Hirrlinger, J.; Kirchhoff, F. Expression of reef coral fluorescent proteins in the central nervous system of transgenic mice. *Mol. Cell. Neurosci.* **2005**, *30*, 291−303.
(61) Sobue, G.; Shuman, S.; Pleasure, D. Schwann cell responses to cyclic AMP: Proliferation, change in shape, and appearance of surface galactocerebroside. *Brain Res.* **1986**, *362*, 23−32.
(62) Yamada, H.; Komiyama, A.; Suzuki, K. Schwann cell responses to forskolin and cyclic AMP analogues: comparative study of mouse and rat Schwann cells. *Brain Res.* **1995**, *681*, 97−104.
(63) Bacallao, K.; Monje, P. V. Opposing Roles of pka and epac in the cAMP-Dependent Regulation of Schwann Cell Proliferation and Differentiation. *PLoS One* **2013**, *8*, No. e82354.
(64) Yokoyama, U.; Patel, H. H.; Lai, N. C.; Aroonsakool, N.; Roth, D. M.; Insel, P. A. The cyclic AMP effector Epac integrates pro- and anti-fibrotic signals. *Proc. Natl. Acad. Sci.* **2008**, *105*, 6386−6391.
(65) Tsubouchi, S.; Kano, E.; Suzuki, H. Demonstration of expanding cell populations in mouse pancreatic acini and islets. *Anat. Rec.* **1987**, *218*, 111−115.
(66) Furth, P. A.; St Onge, L.; Böger, H.; Gruss, P.; Gossen, M.; Kistner, A.; Bujard, H.; Hennighausen, L. Temporal control of gene expression in transgenic mice by a tetracycline-responsive promoter. *Proc. Natl. Acad. Sci.* **1994**, *91*, 9302−9306.

https://dx.doi.org/10.1021/acssensors.9b01941
ACS Sens. XXXX, XXX, XXX−XXX

(67) Feil, R.; Brocard, J.; Mascrez, B.; LeMeur, M.; Metzger, D.; Chambon, P. Ligand-activated site-specific recombination in mice. *Proc. Natl. Acad. Sci.* **1996**, *93*, 10887−10890.
(68) Hitoshi, N.; Ken-ichi, Y.; Jun-ichi, M. Efficient selection for high-expression transfectants with a novel eukaryotic vector. *Gene* **1991**, *108*, 193−199.
(69) Miyoshi, H.; Blömer, U.; Takahashi, M.; Gage, F. H.; Verma, I. M. Development of a self-inactivating lentivirus vector. *J. Virol.* **1998**, *72*, 8150−8157.
(70) Lillo, M. P.; Beechem, J. M.; Szpikowska, B. K.; Sherman, M. A.; Mas, M. T. Design and Characterization of a Multisite Fluorescence Energy-Transfer System for Protein Folding Studies: A Steady-State and Time-Resolved Study of Yeast Phosphoglycerate Kinase †. *Biochemistry* **1997**, *36*, 11261−11272.
(71) Aoki, K.; Matsuda, M. Visualization of small GTPase activity with fluorescence resonance energy transfer-based biosensors. *Nat. Protoc.* **2009**, *4*, 1623.
(72) Sumiyama, K.; Kawakami, K.; Yagita, K. A simple and highly efficient transgenesis method in mice with the Tol2 transposon system and cytoplasmic microinjection. *Genomics* **2010**, *95*, 306−311.
(73) Sano, T.; Kobayashi, T.; Negoro, H.; Sengiku, A.; Hiratsuka, T.; Kamioka, Y.; Liou, L. S.; Ogawa, O.; Matsuda, M. Intravital imaging of mouse urothelium reveals activation of extracellular signal-regulated kinase by stretch-induced intravesical release of ATP. *Physiol. Rep.* **2016**, *4*, No. e13033.

https://dx.doi.org/10.1021/acssensors.9b01941
ACS Sens. XXXX, XXX, XXX−XXX